



Coarse-Grained Modeling of Coronavirus Spike Proteins and ACE2 Receptors

Timothy Leong, Chandhana Voleti and Zhangli Peng*

Richard and Loan Hill Department of Bioengineering, University of Illinois at Chicago, Chicago, IL, United States

We developed coarse-grained models of spike proteins in SARS-CoV-2 coronavirus and angiotensin-converting enzyme 2 (ACE2) receptor proteins to study the endocytosis of a whole coronavirus under physiologically relevant spatial and temporal scales. We first conducted all-atom explicit-solvent molecular dynamics simulations of the recently characterized structures of spike and ACE2 proteins. We then established coarse-grained models using the shape-based coarse-graining approach based on the protein crystal structures and extracted the force field parameters from the all-atom simulation trajectories. To further analyze the coarse-grained models, we carried out normal mode analysis of the coarse-grained models to refine the force field parameters by matching the fluctuations of the internal coordinates with the original all-atom simulations. Finally, we demonstrated the capability of these coarse-grained models by simulating the endocytosis of a whole coronavirus through the host cell membrane. We embedded the coarse-grained models of spikes on the surface of the virus envelope and anchored ACE2 receptors on the host cell membrane, which is modeled using a one-particle-thick lipid bilayer model. The coarse-grained simulations show the spike proteins adopt bent configurations due to their unique flexibility during their interaction with the ACE2 receptors, which makes it easier for them to attach to the host cell membrane than rigid spikes.

Keywords: multiscale modeling, endocytosis, SARS-CoV-2, cell membrane, coarse-graining

INTRODUCTION

Although a significant amount of research effort has been conducted to understand the SARS-CoV-2 coronaviruses and vaccines have been developed the exact infection mechanisms remain unclear [1]. Coronaviruses are spherical viruses with unique surface spikes [2]. The average diameter is about 80–120 nm. The virus is protected by the envelope and nucleocapsid when it is outside the host cell [3]. The RNAs of the virus are enclosed in an envelope with a diameter of roughly 85 nm [1]. The envelope consists of a lipid bilayer and the membrane (M), envelope (E), and spike (S) structural proteins embedded in the bilayer. While membrane proteins, envelope proteins, and the lipid bilayer shape the viral envelope and maintain its size, spike proteins interact with the host cells by binding with surface receptors such as angiotensin-converting enzyme 2 (ACE2) receptors. Cryo-electron microscopy (cryo-EM) and x-ray crystallographic techniques have been applied to reveal the new structures of viral proteins [4–16]. Due to their significance, computational modeling was employed alongside experimental studies to investigate the properties of these proteins [17], but most of these existing computational studies are limited to atomistic length and time scales. In this study, we will

OPEN ACCESS

Edited by:

Ying Li,
University of Connecticut,
United States

Reviewed by:

Baofu Qiao,
Northwestern University,
United States
Zhiqiang Shen,
Oak Ridge National Laboratory (DOE),
United States

*Correspondence:

Zhangli Peng
zhpeng@uic.edu

Specialty section:

This article was submitted to
Biophysics,
a section of the journal
Frontiers in Physics

Received: 15 March 2021

Accepted: 18 May 2021

Published: 04 June 2021

Citation:

Leong T, Voleti C and Peng Z (2021)
Coarse-Grained Modeling of
Coronavirus Spike Proteins and
ACE2 Receptors.
Front. Phys. 9:680983.
doi: 10.3389/fphy.2021.680983

investigate the endocytosis of the whole virus under physiologically relevant spatial and temporal scales by constructing coarse-grained models of the spike proteins and ACE2 receptors.

On the one hand, multiscale coarse-grained models of the whole coronavirus have been developed [15], but they have not been applied to study the endocytosis. In addition, to build a minimal model with enough molecular details, we adopted a more aggressive coarse-graining approach than that used in [15] for both proteins and membranes. On the other hand, the endocytosis of nanoparticles has been extensively studied by computational modeling [18–24], but the endocytosis of coronavirus has not been explored computationally with sufficient molecular details. In the current study, we will explicitly take into account the detailed molecular structures of the spikes and ACE2 rather than modeling them as abstract binding points.

We will focus on establishing the coarse-grained models of the spike proteins and ACE2 receptors. The spikes are unique structures of coronaviruses and are responsible for their distinguishing halo-like surface. A coronavirus particle typically has about 70 spikes on its surface [25]. Each spike consists of three spike proteins (a trimer) and its length is about 20 nm. Each spike protein is made of an S1 head subunit and an S2 stem subunit. The S1 head subunit includes the receptor-binding domain (RBD). Although one spike has three RBDs, only one of them is in the up position for binding [26]. The S2 stem subunit anchors the spike in the viral envelope. Recently, the crystal structure of the SARS-CoV-2 spike protein has been characterized using cryo-EM [PDB ID: 6Vestigial sideband (VSB)] [6], which is responsible for binding to the cell membrane *via* the extracellular domain of the ACE2 receptor (PDB ID: 6M17) [27]. ACE2 receptor is a membrane-bound carboxypeptidase that forms a dimer and serves as the cellular receptor for SARS-CoV-2 [27]. Molecular dynamics (MD) simulations revealed that the spike protein polybasic cleavage sites, which are distributed approximately 10 nm away from the RBD, can enhance the binding affinity between the SARS-CoV-2 RBD and ACE2 [28]. We took this into consideration by using the enhanced binding energy (−177 kcal/mol) between RBD and ACE2 among the predicted values of −50 kcal/mol ~ −177 kcal/mol [28–32].

During the infection, the viral spike proteins first attach to their complementary host cell receptors such as ACE2. Then the host cell protease activates the receptor-attached spike proteins. The virus enters the host cell by either endocytosis or membrane fusion of the viral envelope with the host membrane, depending on the availability of the host cell proteases [33]. One of our goals is to simulate the endocytosis by coarse-grained modeling and explicit consideration of the structures of spike and receptor proteins. We will focus on the endocytosis simulation in this study and extend the model to study membrane fusion in the future.

Since the coronavirus is more than 80 nm, all-atom molecular dynamics simulation is prohibitively expensive, not to mention the long-time scale of the endocytosis. Instead, we will apply a multiscale modeling approach. We will conduct all-atom MD

simulations of the spike protein and the ACE2 receptors based on their recently characterized crystal structures. Then we will build coarse-grained models of these proteins using the all-atom simulation trajectories. After we demonstrate that the coarse-grained model share similar structural properties with the original all-atom proteins by matching fluctuations, we will construct a whole virus model with a realistic number of spike proteins, and conduct simulations of the endocytosis process of the virus to investigate the cell entry mechanisms. In addition, we developed automated scripts and MATLAB code for establishing these CG models and conducting normal mode analysis. We made them publicly available so that other users can repeat and modify these models.

MATERIALS AND METHODS

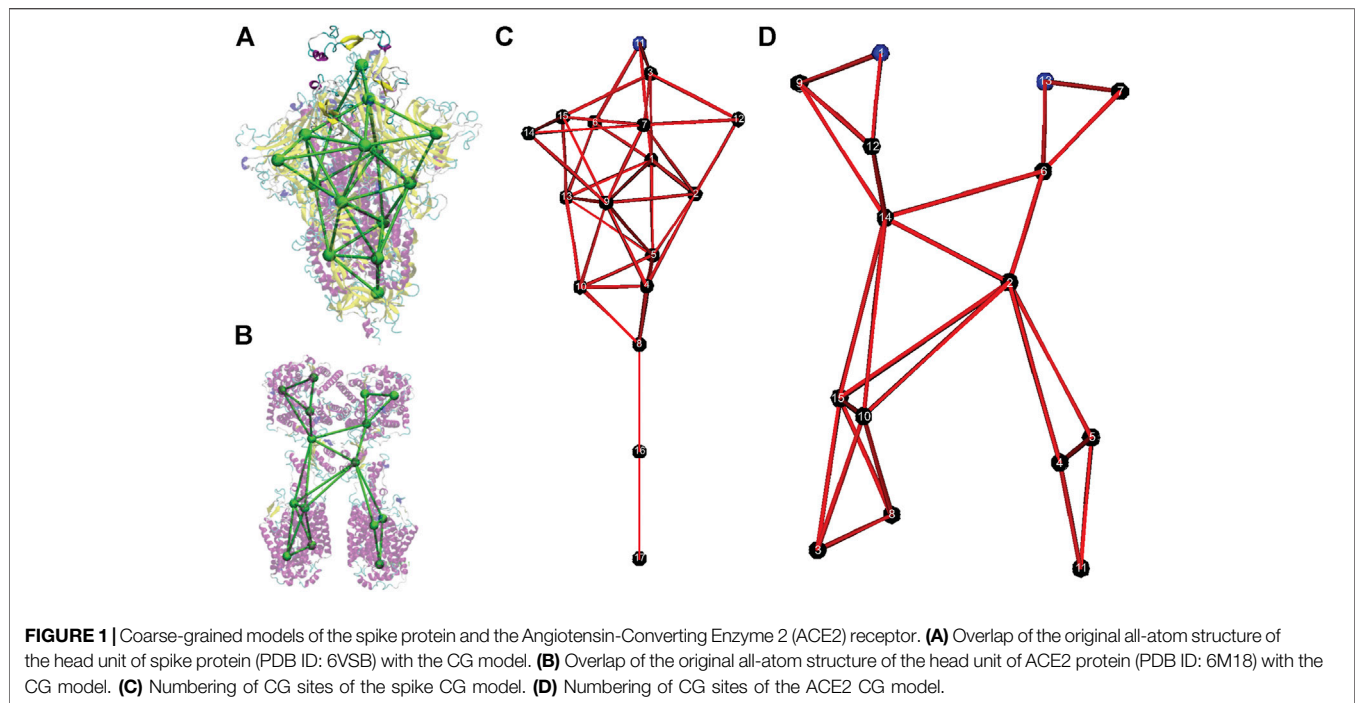
All-Atom Molecular Dynamics Simulations

All-atom MD simulations of the spike protein and ACE2 receptor were conducted using Nanoscale Molecular Dynamics (NAMD) [34]. Explicit solvent is used in order to capture the accurate fluctuations of the structure in equilibrium. A standard protocol is applied. Minimization and annealing processes were carried out first and then equilibrium simulation with the backbone fixed were done before production MD simulations were run. Both the fully-glycosylated full-length spike protein model (**Supplementary Figure S1** in the Supplementary Material) and spike protein head S1 subunit model (**Figure 1A**) were conducted by following the procedure described in [35]. The simulation of the S1 subunit model is used to extract the force field parameters of the bonds and angles in the S1 subunit, and the simulation of the full-length spike protein model is used to estimate the bond and angle coefficients for the stem S2 subunit. A typical simulation box is 25 by 25 by 38 nm and about 2.3 million atoms were simulated for 20 ns. All-atom MD and CG simulations were conducted on the supercomputer Theta in Argonne Leadership Computing Facility (ALCF) in the Argonne National Lab.

Shape-Based Coarse-Graining and Coarse Grained Simulations

We utilized a technique called the Shape-Based Coarse Graining (SBCG) approach to develop the CG models, where large-scale motions of organic/biological molecules are represented using as few spherical CG sites (beads) as possible [36]. This decreases computational demand significantly when performing molecular dynamics simulations. When it comes to the force-field equation, atoms are substituted with CG beads. “Intramolecular” bonds between CG beads are established if the CG beads are within a certain distance of each other, or if the all-atom domains that comprise the CG beads are contiguously connected by intramolecular bonds.

We applied the SBCG tool in Visual Molecular Dynamics (VMD) to construct the coarse-grained model [37]. First, the CG sites and bonded interactions (bonds and angles) were established based on the original all-atom structures. The coefficients of



Lennard-Jones (LJ) potential and the bonded interactions were extracted based on all-atom MD simulation trajectories. Specifically, an initial guess of the coefficients of bonded interactions was made by matching the root mean square displacement (RMSD) of internal coordinates, such as bond lengths and angles. Then iterations of refinements were made through CGMD simulations and normal mode analysis [38]. Detailed steps are shown in the **Supplementary Material**. In addition, we also developed an automated Tool Command Language (TCL) script for this procedure (“To-CG-File.tcl”) within the **Supplementary Material**. The following classical intramolecular and intermolecular interactions without dihedrals were used

$$V = \sum_{\text{bonds } k} \frac{K_{b,k}}{2} (R_k - R_{0,k})^2 + \sum_{\text{angles } k} \frac{K_{\theta,k}}{2} (\theta_k - \theta_{0,k})^2 + \sum_{\text{beads } i,j} 4E_{ij} \left[\left(\frac{\sigma_{ij}}{r_{ij}} \right)^{12} - \left(\frac{\sigma_{ij}}{r_{ij}} \right)^6 \right] + \sum_{\text{beads } i,j} \frac{q_i q_j}{4\pi\epsilon\epsilon_0 r_{ij}} \quad (1)$$

where $E_{ij} = (E_i \times E_j)^{1/2}$, $\sigma_{ij} = (\sigma_i + \sigma_j)/2.0$. The first term in **Eq. 1** represents the energy associated with the harmonic oscillation of a bond connecting two beads. $K_{b,k}$ is the proportionality constant for the harmonic oscillator, and $R_{0,k}$ is the equilibrium distance of the bond, or, the distance where the elastic force is zero for bond k . The 2nd term represents the energy associated with the harmonic oscillation of an angle between the position vectors of two beads that are bonded to a common bead. $K_{\theta,k}$ is the proportionality constant, and $\theta_{0,k}$ is the equilibrium angle between the three beads for angle k . Energy arising from electrostatic interactions is modeled

through Coulombic potential energy and the Van der Waals interaction is modeled using the 6–12 LJ potential. r_{ij} is the distance between beads i and j , and q_i and q_j are the charges of beads i and j , respectively. ϵ_0 is the vacuum permittivity constant and ϵ is the relative permittivity of the medium that beads i and j exist in. σ_{ij} represents the Van der Waals radius of the pair of beads i and j , or, the distance where the LJ potential is zero. E_{ij} is a proportionality constant representing the minima of the LJ potential energy graph for the paired beads i and j , and is proportional to the maximum strength of the attraction between beads i and j . LJ potentials prevent the overlapping or penetrating of neighboring CG sites. The equation sums up all of the individual energies obtained from every intramolecular bond, intramolecular bond angle, and every combinatorial pair of beads that exist in the molecule. In addition to the force field approximations, the following Langevin equation is used to describe the motions of the CG beads

$$m \frac{\partial^2 \mathbf{r}}{\partial t^2} = \mathbf{F} - m\gamma \frac{\partial \mathbf{r}}{\partial t} + \chi \psi(t) \quad (2)$$

where \mathbf{F} is the force imparted on the bead by other beads in the system, \mathbf{r} is the position of the bead, m is the mass of the bead, γ is the damping coefficient of the solvent the bead is in, and χ is a fluctuation-dissipation theorem function of the form $\chi = (2\gamma k_B T/m)^{1/2}$, where k_B is the Boltzmann constant. $\psi(t)$ is a Gaussian process used to simulate Brownian motion. As $\partial^2 \mathbf{r} / \partial t^2$ would represent the acceleration of the bead, then this Langevin equation describes the motion of the bead after accounting for fluid viscous friction and thermal fluctuations.

The CG simulations of individual spike proteins and ACE2 receptors were carried out in NAMD for refinement of the force field parameters.

The detailed procedure is given in the **Supplementary Material** for building the CG model based on all-atom MD simulations in VMD and converting it to the format of molecule files that can be used in CG simulations of endocytosis using Large-scale Atomic/Molecular Massively Parallel Simulator (LAMMPS) [39].

Normal Mode Analysis

We also wrote a Matlab code to conduct the normal mode analysis (NMA) [38] of the two CG models. We constructed the Hessian matrix $\nabla^2 E$ (E is the total energy) based on bond and angle interactions

$$|\nabla^2 E - \lambda \mathbf{M}| = 0 \quad (3)$$

where \mathbf{M} is the mass matrix and $\lambda = \omega^2$ is the eigenvalue (ω is the vibration frequency). We diagonalized the mass weighted Hessian matrix to obtain eigenvalues and eigenvectors. The fluctuations of the CG bead coordinates are given as

$$\langle \Delta x_k^2 \rangle = \sum_{i=1}^{3N-6} \frac{k_B T}{M_k \omega^2} |y_{ki}|^2 \quad (4)$$

The mean square displacement (MSD) of the internal coordinates can be written as function of eigenvalues and eigenvectors as [38].

$$\langle \Delta \phi_j^2 \rangle = \sum_{i=1}^{3N-6} \frac{k_B T}{\omega^2} \sum_{k=1}^{3N} |B_{jk} M_k^{-1/2} y_{kj}|^2 \quad (5)$$

where $\omega^2 = \lambda$ and \mathbf{y} is the eigenvector and \mathbf{B} is the Wilson matrix relating the CG bead coordinates to the internal coordinate as $\Delta \phi = \mathbf{B} \Delta \mathbf{x}$ [38].

Setup of Endocytosis Coarse-Grained Simulations

We modeled the envelope of the virus as a rigid sphere with a diameter of 85 nm. Seventy-two spikes are embedded in the envelope in our model. The end CG sites (CG site 17 in **Figure 1C**) of the spike stems are anchored to the envelope. Morse bonds are formed between the receptor binding site (CG site 11 **Figure 1C**) of the spike and the binding sites (CG sites 1 and 13 in **Figure 1D**) of the ACE2 protein when they get close to each other. Only one receptor binding site is modeled on each spike, as the crystal structure of the spike has only one receptor binding site up [26]. Two binding sites on each ACE2 receptor were modeled. The virus is given an initial small velocity towards the cell membrane to initiate the endocytosis process. Body temperature is used for all simulations, and a simulation box of 800 by 800 by 1600 nm is applied with the periodic boundary condition. While there is no direct measurement of absolute ACE2 surface densities and only relative ACE2 expressions were measured [40, 41], Chen et al. measured a density of 480–640/ μm^2 for receptors of various species [42]. We used a surface density of 300/ μm^2

which is about 1/10 of the surface density of the spike on the envelope (3,260/ μm^2). This value was also used in a recent study to quantify the adhesive strength between the SARS-CoV-2 spike proteins and the human receptor ACE2 [43].

We applied the one-particle-thick lipid bilayer model [44], which we developed as a LAMMPS package [45], to simulate a flat cell membrane patch with ACE2 proteins embedded. It gives a bending rigidity of 50 $k_B T$, and ACE2 proteins can diffuse freely on the surface of the fluctuating cell membrane. All the CG simulations of endocytosis were carried out in LAMMPS.

We used the Berendsen thermostat and barostat to control the temperature and membrane tension. The temperature is set to $T = 0.23 \epsilon/k_B$ for all the particles in the simulations, where ϵ is the energy depth in the one-particle-thick lipid bilayer. We controlled the membrane tension to zero by setting the coupled XYZ pressure to zero. Because the out-of-plane stress of the membrane is always zero, and the membrane is curved in 3D due to deformation, the coupled XYZ pressure is linearly proportional to the membrane tension.

The binding energy between the spike RBD and ACE2 is modeled using the Morse breakable bond as

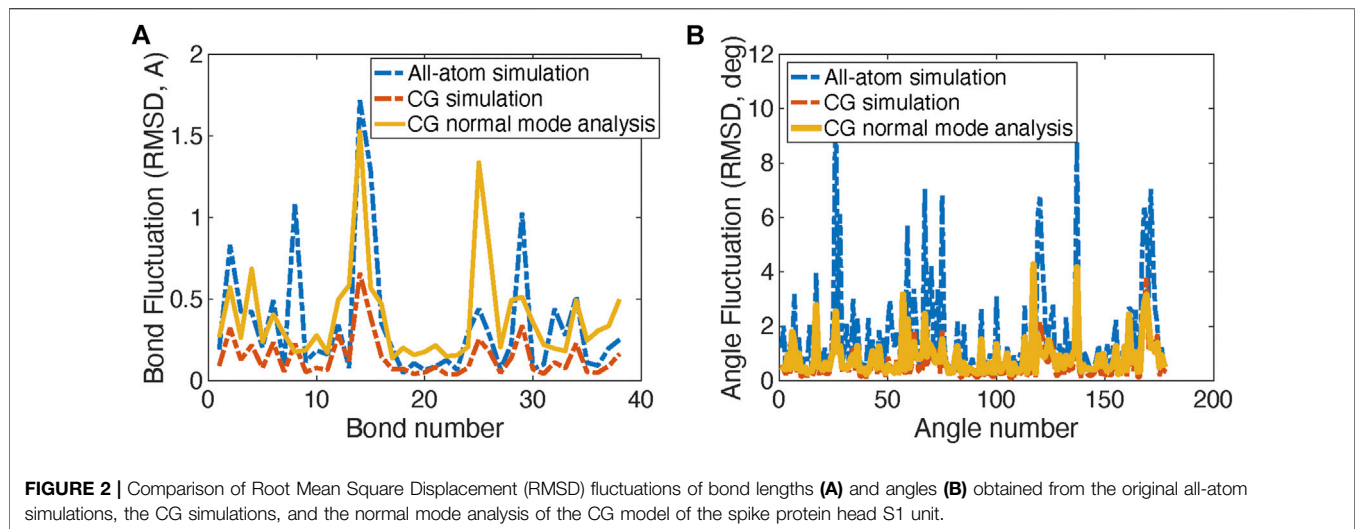
$$E = D \left[1 - e^{-\alpha(r-r_0)} \right]^2 \quad (6)$$

with an energy well depth of $D = 68 \epsilon$, which gives a physical value of 177 kcal/mol obtained from all-atom simulations [28], and $\alpha = 1.0$, $r_0 = 1$ nm. We used Morse breakable bonds instead of Morse pair interactions because pair interactions can cause clustering of ACE2 receptors, as many ACE2 receptors can bind to the same spike at the same time [18]. This unphysical problem can be solved by using LAMMPS commands “fix bond/create” and “fix bond/break”. We set the maximum number of bonds that can be formed for the spike RBD from ACE2 to be one. The cutoff for Morse bond formation in “fix bond/create” is set to 20 nm, and the cutoff for Morse bond break in “fix bond/break” is set to 28 nm. By using the command “fix bond/break”, we not only make the simulation of binding/unbinding more realistic, but also avoid numerical instability due to excessive bond stretch. Because the attraction branch of Morse potential near the cutoff distance is weak, after the bond is formed the bond can be stretched beyond the ghost atom cutoff length in LAMMPS in some cases, leading to errors of missing atoms in multiple CPU simulations. With “fix_bond/break”, the bond will break if it is longer than 28 nm before it reaches the ghost atom cutoff length, which is set to 30 nm in the simulations.

RESULTS

Overview of the Coarse-Grained Models

Although different resolutions of coarse-graining can be developed by using the SBCG approach, we focused on the minimal model with a small number of CG sites. The CG models for the SARS-CoV-2 spike protein and the ACE2 receptor are shown in **Figure 1B**. In **Figure 1A** and **Figure 2B**, the CG models are superimposed on top of their respective all-atom structures, and only the head S1 subunit is



shown for the spike protein. The all-atom systems are colored based on their secondary structures.

The CG model of the spike protein has 17 CG sites. Sites 1–15 represent the S1 head subunit and sites 16 and 17 present the S2 stem subunit. Within the S1 subunit, CG site 11 represents the receptor binding domain (RBD) in the original crystal structure (PDB: 6VSB), and CG sites 3 and 15 present the hidden RBDs. CG sites 6, 12, and 14 represent the outer beta sheets domains of each spike protein in the trimer. In the S2 subunit, CG site 17 is anchored in the viral envelope, and CG site eight is the connecting region between S1 and S2 subunits.

The CG model of the ACE2 receptor has 15 CG sites. CG sites 3, 4, 5, 8, 10, 11, and 15 represent the transmembrane domains, while CG sites 1 and 13 represent two binding sites for the spike protein.

Parameters of the Coarse-Grained Model

The CG parameters in Eq. 1, such as bond coefficients and initial lengths, are listed as **Supplementary Tables S1–S8** in the Supplementary Material for the SARS-CoV-2 spike protein and the ACE2 receptor. Note that only bond and angle interactions are used as shown in Eq. 1, while dihedral angles are not included in this shape-based coarse-graining approach.

Note that the bonded coefficients of the S1 head subunit are obtained from the all-atom simulations of the S1 head subunit, while the bonded coefficients of S2 subunits are obtained from the fully-glycosylated full-length spike protein model (**Supplementary Figure S1** in the Supplementary Material).

The comparison RMSDs of the original all-atom simulations with the CG models for bond length and angles are shown in **Figure 2A**. **Figure 2B** shows the fluctuation magnitudes of the CG model match well with the original all-atom model.

Normal mode analysis of the coarse-grained model

Normal mode analysis (NMA) is also applied to calculate the fluctuations and vibration modes of the CG models. In **Figure 2B**,

the fluctuations (yellow curves) obtained by NMA match well with the all-atom model. The fluctuations calculated from NMA are different from the fluctuations obtained from direction CG simulation of the same model due to the anharmonic effect in the direct CG simulations. In addition, the first three vibration modes of the spike S1 head unit are shown in **Figure 3**. The 1st and 2nd modes involve the motions of the RBD site in two horizontal directions, respectively, and the 3rd mode involves the motion of one of the three exterior beta sheet domains.

Modeling of the Endocytosis of the Coronavirus.

After we established the CG models of the spike protein and ACE2 protein, we applied them to simulate the endocytosis of a whole coronavirus. As shown in **Figure 4A**, we modeled the virus envelope as a rigid sphere with a diameter of 85 nm. The CG models of the spike proteins (red) are distributed on the surface of the virus with the stems embedded in the viral envelope (grey). The RBD binding sites of the spike proteins (CG site 11 in **Figure 1A**) are highlighted as blue. The transmembrane domain CG sites of the ACE2 proteins (green) are embedded in the host cell membrane (orange). The host cell membrane is modeled by using the one-particle-thick bilayer model [44, 45]. The same interaction is applied between the cell membrane particles and the CG particles of the transmembrane domains of ACE2 so that the ACE2 proteins are anchored in the cell membrane with the right orientation as shown in **Figure 4A**. The binding sites of the ACE2 proteins are also shown as blue. The depth of the energy well ϵ of the pair interaction in the one-particle-thick model is set to about 5.0 times thermal energy ($k_B T$) and the characteristic length and the cutoff length are set to 4 and 10.4 nm so that the membrane self-assembled into a one-particle-thick layer with the fluid behavior and bending rigidity of $50 k_B T$. The attraction and repulsive parameters $\eta = 2$ and $\zeta = 4$, and the bending parameter $\mu = 3$ (see Fu et al. [45]).

As shown in **Figures 4C,D**, the ACE2 proteins can diffuse on the fluctuating cell membrane with the correct orientations. The

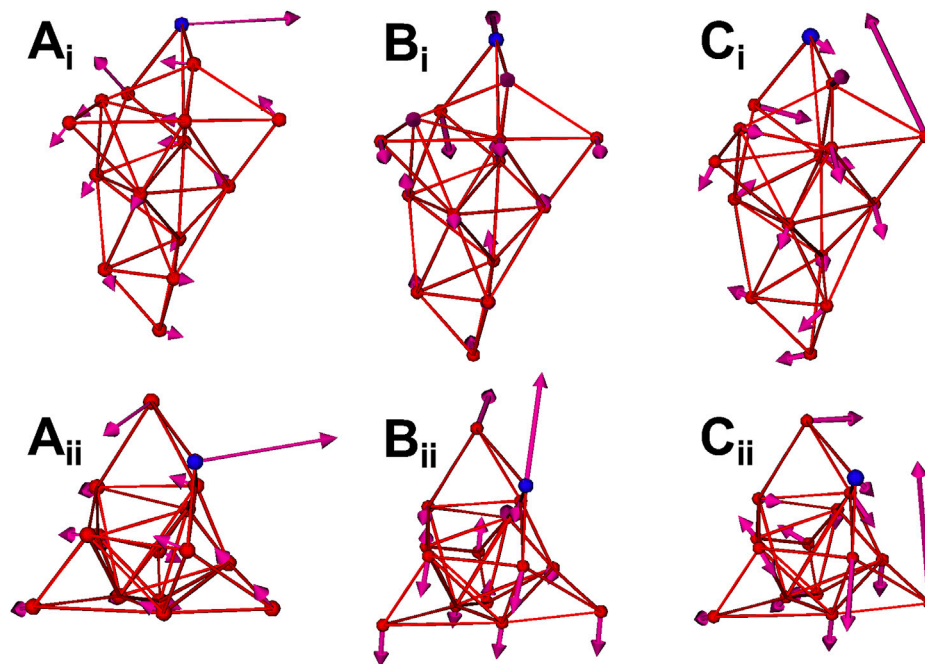


FIGURE 3 | The first three normal modes of the spike CG model. **(Ai)** 1st mode (**side view**). **(Aii)** 1st mode (**top view**). **(Bi)** 2nd mode (**side view**). **(Bii)** 2nd mode (**top view**). **(Ci)** 3rd mode (**side view**). **(Cii)** 3rd mode (**top view**). The RBD site (CG site 11) is highlighted as blue.

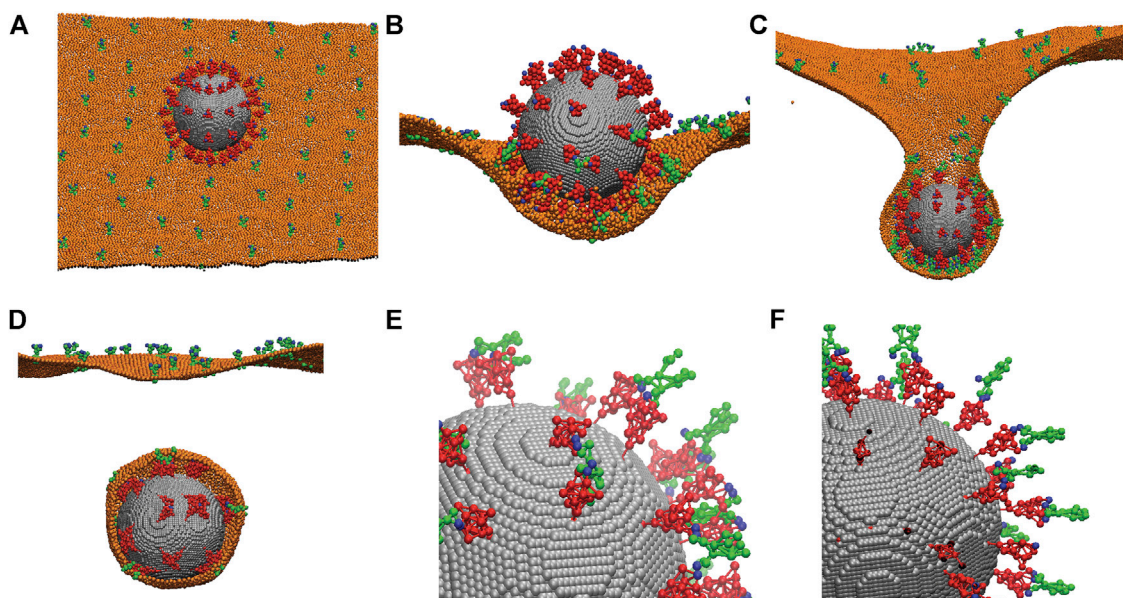


FIGURE 4 | Simulations of the endocytosis of a whole virus by incorporating the CG models of the spike protein and the ACE2 receptor. **(A)** A CG model of the whole virus with 72 distributed spike proteins (red) anchored on its viral envelope (grey). The spike proteins are modeled using the CG model described in **Figure 1**. ACE2 proteins (green) are anchored in the host cell membrane (orange). Both the binding sites of the spike proteins and ACE2 proteins are marked as blue. **(B)** The initial attachment of the virus to the fluctuating cell membrane. **(C)** The progress of the endocytosis due to spike-ACE2 interaction. **(D)** Separation of the membrane-bounded virus from the host cell membrane. Only half of the cell membrane is shown in **(B, C, D)** for revealing the interior virus and interactions. **(E)** A close view of the interactions between the spike proteins (red) and ACE2 receptors (green) through their binding sites (blue). Most ACE2 receptors bind to two spikes. Membrane is not shown. **(F)** The same as **(E)** except the ACE2 receptors and spikes are modeled as rigid bodies without flexibility. All ACE2 bind to one spike only. Membrane is not shown.

Berendsen thermostat and barostat are used to maintain a constant membrane temperature and zero membrane tension. The rigid body dynamics in LAMMPS is employed for the viral envelope, and the NVE integrator with Langevin thermostats is employed for the dynamics of spike and ACE2 proteins under the same temperature as the membrane. The interaction between the spike RBD sites and the ACE2 binding sites is simulated by breakable Morse bonds. The binding energy between the spike and ACE2 is set to -177 kcal/mol, obtained from the literature for spike-ACE2 interaction [28–32].

When the virus is initially attached to the cell membrane, the spike proteins at the bottom surface of the virus bind to the ACE2 proteins and are deformed due to their structure flexibility as shown in **Figure 4B**, while the spike proteins on the top surface remain much less deformed, although they vibrate due to thermal fluctuations. After more ACE2 proteins bind to the spikes, the virus is engulfed by the cell membrane. This eventually leads to the necking and rupture of the cell membrane as shown in **Figures 4C,D**. Our simulations show that due to the flexibility of the spike proteins and their actual surface density, it is possible for the two spikes to bend significantly to bind to the same ACE2 receptor as shown in **Figure 4E**. Our simulations show that this is not possible if the spike and ACE2 proteins are modeled as rigid structures, and one spike can only bind to one ACE2 as shown in **Figure 4F**. Therefore, it is critical to consider the realistic flexibility of the spike and ACE2 proteins in the simulations, as also demonstrated in all-atom MD simulations [46–48].

CONCLUSIONS AND DISCUSSIONS

We developed the CG models of the spike proteins and ACE2 receptors using the shape-based coarse-graining approach. The force field parameters are obtained from the all-atom simulations by matching the fluctuations. Then these CG models are incorporated into LAMMPS to simulate the binding of the spike proteins with the ACE2 receptors during the endocytosis of a whole virus. We found that the realistic structure flexibility of the spike proteins and ACE2 proteins is critical for better interaction between these two proteins. For example, our results showed that two spike proteins can easily bind to one ACE2 receptor due to significant bending deformation.

Besides endocytosis, the coronavirus can enter the host cell by membrane fusion. To model the membrane fusion process in a future study, we will need to consider the viral envelope as a flexible membrane using the one-particle-thick lipid bilayer model. As the connection between the S1 and S2 subunits is cleaved and the S1 head subunit is removed from the virus during the membrane fusion process, we also need to refine the CG model to incorporate this breakable bond mechanism.

In summary, we simulated the endocytosis of the whole coronavirus with minimal atomistic details of its spike proteins and corresponding ACE2 receptors. Although the resolution is coarse and the coarse-graining is aggressive, it

can help us understand the biophysical behavior of the coronavirus at large temporal and spatial scales beyond typical atomistic simulations. Furthermore, the CG resolutions can be refined if needed through the same procedure by using the scripts provided in the **Supplementary Material**.

DATA AVAILABILITY STATEMENT

The original contributions presented in the study are included in the article/**Supplementary Material**, further inquiries can be directed to the corresponding author.

AUTHOR CONTRIBUTIONS

ZP constructed the cell membrane CG model, the CG virus using the SARS-CoV-2 and ACE2 CG models, and performed MD simulations with the aforementioned CG models in LAMMPS. TL designed the coarse-graining program to convert the all-atom SARS-CoV-2 and ACE2 proteins into their CG models, and designed the program to extract the bonding parameters from the CG models and convert them into a LAMMPS-compatible format. TL was also responsible for patching a technical issue that impeded CG model creation. CV designed the normal mode analysis program and performed normal mode analyses on all aforementioned CG models.

FUNDING

ZP acknowledge the funding support from NSF Grant No. CBET-1948347. TL is supported through the Research Experiences for Undergraduates (REU) supplement of NSF CBET-1948347. CV is supported by the Guaranteed Paid Internship Program (GPIP) from University of Illinois at Chicago. This research used resources of the Argonne Leadership Computing Facility, which is a DOE Office of Science User Facility supported under Contract DE-AC02-06CH11357.

ACKNOWLEDGMENTS

All-atom MD and CG simulations were conducted on the supercomputer Theta in Argonne Leadership Computing Facility (ALCF) in the Argonne National Lab under Director's Discretionary (DD) allocation Modeling Corona Virus.

SUPPLEMENTARY MATERIAL

The Supplementary Material for this article can be found online at: <https://www.frontiersin.org/articles/10.3389/fphy.2021.680983/full#supplementary-material>

REFERENCES

- He F, Deng Y, and Li W. Coronavirus Disease 2019: What We Know? *J Med Virol* (2020). 92(7):719–25. doi:10.1002/jmv.25766
- Goldsmith CS, Tatti KM, Ksiazek TG, Rollin PE, Comer JA, Lee WW, et al. Ultrastructural Characterization of SARS Coronavirus. *Emerg Infect Dis* (2004). 10(2):320–6. doi:10.3201/eid1002.030913
- Godet M, L'Haridon R, Vautherot J-F, and Laude H. TGEV corona Virus ORF4 Encodes a Membrane Protein that Is Incorporated into Virions. *Virology* (1992). 188(2):666–75. doi:10.1016/0042-6822(92)90521-p
- Andersson R. University Decentralization as Regional Policy: the Swedish experiment. *J Econ Geogr* (2004). 4(4):371–88. doi:10.1093/jeg/4.4.371
- Berman H, Henrick K, and Nakamura H. Announcing the Worldwide Protein Data Bank. *Nat Struct Mol Biol* (2003). 10(12):980. doi:10.1038/nsb1203-980
- Berman HM. The Protein Data Bank. *Nucleic Acids Res* (2000) 28(1):235–42. doi:10.1093/nar/28.1.235
- Frick DN, Viridi RS, Vuksanovic N, Dahal N, and Silvaggi NR. Molecular Basis for ADP-Ribose Binding to the Mac1 Domain of SARS-CoV-2 Nsp3. *Biochemistry* (2020) 59(28):2608–15. doi:10.1021/acs.biochem.0c00309
- Hillen HS, Kocik G, Farnung L, Dienemann C, Tegunov D, and Cramer P. Structure of Replicating SARS-CoV-2 Polymerase. *Nature* (2020) 584(7819): 154–6. doi:10.1038/s41586-020-2368-8
- Kern DM, Sorum B, Mali SS, Hoel CM, Sridharan S, Remis JP, et al. *Cryo-EM Structure of the SARS-CoV-2 3a Ion Channel in Lipid Nanodiscs*. *bioRxiv* (2020) [Preprint]. doi:10.1101/2020.06.17.156554
- Rut W, Lv Z, Zmudzinski M, Patchett S, Nayak D, Snipas SJ, et al. *Activity Profiling and Structures of Inhibitor-Bound SARS-CoV-2-PLpro Protease Provides a Framework for Anti-COVID-19 Drug Design*. *bioRxiv* (2020) [Preprint]. doi:10.1101/2020.04.29.068890
- Shang J, Ye G, Shi K, Wan Y, Luo C, Aihara H, et al. Structural Basis of Receptor Recognition by SARS-CoV-2. *Nature* (2020) 581(7807):221–4. doi:10.1038/s41586-020-2179-y
- Yan R, Zhang Y, Li Y, Xia L, Guo Y, and Zhou Q. Structural basis for the recognition of SARS-CoV-2 by full-length human ACE2. *Science* (2020) 367(6485):1444–1448. doi:10.1126/science.abb2762
- Surya W, Li Y, and Torres J. Structural Model of the SARS Coronavirus E Channel in LMPG Micelles. *Biochim Biophys Acta (Bba) - Biomembranes* (2018) 1860(6):1309–17. doi:10.1016/j.bbmem.2018.02.017
- Walls AC, Park Y-J, Tortorici MA, Wall A, McGuire AT, and Veerles D. Structure, Function, and Antigenicity of the SARS-CoV-2 Spike Glycoprotein. *Cell* (2020) 183(6):1735. doi:10.1016/j.cell.2020.11.032
- Yu A, Pak AJ, He P, Monje-Galvan V, Casalino L, Gaieb Z, et al. A Multiscale Coarse-Grained Model of the SARS-CoV-2 Virion. *Biophys J* (2021) 120(6): 1097–1104. doi:10.1016/j.bpj.2020.10.048
- Zhang L, Lin D, Sun X, Curth U, Drosten C, Sauerhering L, et al. Crystal Structure of SARS-CoV-2 Main Protease Provides a Basis for Design of Improved α -ketoamide Inhibitors. *Science* (2020) 368(6489):409–12. doi:10.1126/science.abb3405
- Jaimes JA, André NM, Chappie JS, Millet JK, and Whittaker GR. Phylogenetic Analysis and Structural Modeling of SARS-CoV-2 Spike Protein Reveals an Evolutionary Distinct and Proteolytically Sensitive Activation Loop. *J Mol Biol* (2020) 432(10):3309–25. doi:10.1016/j.jmb.2020.04.009
- Shen Z, Ye H, Yi X, and Li Y. Membrane Wrapping Efficiency of Elastic Nanoparticles during Endocytosis: Size and Shape Matter. *ACS Nano* (2018) 13(1):215–28. doi:10.1021/acs.nano.8b05340
- Shen Z, Ye H, and Li Y. Understanding Receptor-Mediated Endocytosis of Elastic Nanoparticles through Coarse Grained Molecular Dynamic Simulation. *Phys Chem Chem Phys* (2018) 20(24):16372–85. doi:10.1039/c7cp08644j
- Shen Z, Ye H, Kröger M, and Li Y. Aggregation of Polyethylene Glycol Polymers Suppresses Receptor-Mediated Endocytosis of PEGylated Liposomes. *Nanoscale* (2018) 10(9):4545–60. doi:10.1039/c7nr09011k
- Richards DM, and Endres RG. Target Shape Dependence in a Simple Model of Receptor-Mediated Endocytosis and Phagocytosis. *Proc Natl Acad Sci USA* (2016) 113(22):6113–8. doi:10.1073/pnas.1521974113
- Li Y, Kröger M, and Liu WK. Endocytosis of PEGylated Nanoparticles Accompanied by Structural and Free Energy Changes of the Grafted Polyethylene Glycol. *Biomaterials* (2014) 35(30):8467–78. doi:10.1016/j.biomaterials.2014.06.032
- Gao H, Shi W, and Freund LB. From the Cover: Mechanics of Receptor-Mediated Endocytosis. *Proc Natl Acad Sci* (2005) 102(27):9469–74. doi:10.1073/pnas.0503879102
- Doherty GJ, and McMahon HT. Mechanisms of Endocytosis. *Annu Rev Biochem* (2009) 78(1):857–902. doi:10.1146/annurev.biochem.78.081307.110540
- Neuman BW, Kiss G, Kunding AH, Bhella D, Baksh MF, Connelly S, et al. A Structural Analysis of M Protein in Coronavirus Assembly and Morphology. *J Struct Biol* (2011) 174(1):11–22. doi:10.1016/j.jsb.2010.11.021
- Wrapp D, Wang N, Corbett KS, Goldsmith JA, Hsieh C-L, Abiona O, et al. Cryo-EM Structure of the 2019-nCoV Spike in the Prefusion Conformation. *Science* (2020) 367(6483):1260–3. doi:10.1126/science.abb2507
- Yan R, Zhang Y, Li Y, Xia L, Guo Y, and Zhou Q. Structural Basis for the Recognition of SARS-CoV-2 by Full-Length Human ACE2. *Science* (2020) 367(6485):1444–8. doi:10.1126/science.abb2762
- Qiao B, and Olvera de la Cruz M. Enhanced Binding of SARS-CoV-2 Spike Protein to Receptor by Distal Polybasic Cleavage Sites. *ACS Nano* (2020) 14(8): 10616–23. doi:10.1021/acsnano.0c04798
- Ali A, and Vijayan R. Dynamics of the ACE2–SARS-CoV-2/sars-CoV Spike Protein Interface Reveal Unique Mechanisms. *Scientific Rep* (2020) 10(1). doi:10.1038/s41598-020-71188-3
- He J, Tao H, Yan Y, Huang S-Y, and Xiao Y. Molecular Mechanism of Evolution and Human Infection with SARS-CoV-2. *Viruses* (2020) 12(4):428. doi:10.3390/v12040428
- Mercurio I, Tragni V, Busto F, De Grassi A, and Pierri CL. Protein Structure Analysis of the Interactions between SARS-CoV-2 Spike Protein and the Human ACE2 Receptor: from Conformational Changes to Novel Neutralizing Antibodies. *Cell. Mol. Life Sci.* (2020) 78(4):1501–22. doi:10.1007/s00018-020-03580-1
- Spinello A, Saltalamacchia A, and Magistrato A. Is the Rigidity of SARS-CoV-2 Spike Receptor-Binding Motif the Hallmark for Its Enhanced Infectivity? Insights from All-Atom Simulations. *J Phys Chem Lett* (2020)11(12): 4785–4790. doi:10.1021/acs.jpclett.0c01148
- Simmons G, Zmora P, Gierer S, Heurich A, and Pöhlmann S. Proteolytic Activation of the SARS-Coronavirus Spike Protein: Cutting Enzymes at the Cutting Edge of Antiviral Research. *Antiviral Res* (2013) 100(3):605–14. doi:10.1016/j.antiviral.2013.09.028
- Phillips JC, Hardy DJ, Maia JDC, Stone JE, Ribeiro JV, Bernardi RC, et al. Scalable Molecular Dynamics on CPU and GPU Architectures with NAMD. *J Chem Phys* (2020) 153(4):044130. doi:10.1063/5.0014475
- Woo H, Park S-J, Choi YK, Park T, Tanveer M, Cao Y, et al. Developing a Fully Glycosylated Full-Length SARS-CoV-2 Spike Protein Model in a Viral Membrane. *J Phys Chem B* (2020) 124(33):7128–37. doi:10.1021/acs.jpcc.0c04553
- Arkhypov A, Schulten K, Freddolino P, Ying Y, Shih A, and Chen Z. *Coarse-Graining of Condensed Phase and Biomolecular Systems*. Boca Raton, FL: CRC Press (2008). p. 299–315. doi:10.1201/9781420059564_ch20 Application of Residue-Based and Shape-Based Coarse-Graining to Biomolecular Simulations.
- Humphrey W, Dalke A, and Schulten K. VMD: Visual Molecular Dynamics. *J Mol Graphics* (1996) 14(1):33–8. doi:10.1016/0263-7855(96)00018-5
- Brooks BR, Jane?? Da., and Karplus M. Harmonic Analysis of Large Systems. I. Methodology. *J Comput Chem* (1995) 16(12):1522–42. doi:10.1002/jcc.540161209
- Plimpton S. Fast Parallel Algorithms for Short-Range Molecular Dynamics. *J Comput Phys* (1995) 117(1):1–19. doi:10.1006/jcph.1995.1039
- Al-Benna S. Association of High Level Gene Expression of ACE2 in Adipose Tissue with Mortality of COVID-19 Infection in Obese Patients. *Obes Med* (2020) 19:100283. doi:10.1016/j.obmed.2020.100283
- Zhang L, Han X, and Shi Y. Comparative Analysis of SARS-CoV-2 Receptor ACE2 Expression in Multiple Solid Tumors and Matched Non-diseased Tissues. *Infect Genet Evol* (2020) 85:104428. doi:10.1016/j.meegid.2020.104428
- Chen Y, Munteanu AC, Huang Y-F, Phillips J, Zhu Z, Mavros M, et al. Mapping Receptor Density on Live Cells by Using Fluorescence Correlation Spectroscopy. *Chem Eur J* (2009) 15(21):5327–36. doi:10.1002/chem.200802305
- Ponga M. Quantifying the Adhesive Strength between the SARS-CoV-2 S-Proteins and Human Receptor and its Effect in Therapeutics. *Scientific Rep* (2020) 10(1). doi:10.1038/s41598-020-74189-4

44. Yuan H, Huang C, Li J, Lykotrafitis G, and Zhang S. One-particle-thick, Solvent-free, Coarse-Grained Model for Biological and Biomimetic Fluid Membranes. *Phys Rev E* (2010) 82(1). doi:10.1103/physreve.82.011905
45. Fu S-P, Peng Z, Yuan H, Kfoury R, and Young Y-N. Lennard-Jones Type Pair-Potential Method for Coarse-Grained Lipid Bilayer Membrane Simulations in LAMMPS. *Computer Phys Commun* (2017) 210:193–203. doi:10.1016/j.cpc.2016.09.018
46. Barros EP, Casalino L, Gaieb Z, Dommer AC, Wang Y, Fallon L, et al. The Flexibility of ACE2 in the Context of SARS-CoV-2 Infection. *Biophys J* (2020) 120(6):1072–1084. doi:10.1101/2020.09.16.300459
47. Pierrri CL. SARS-CoV-2 Spike Protein: Flexibility as a New Target for Fighting Infection. *Signal Transduction Targeted Ther* (2020) 5(1). doi:10.1038/s41392-020-00369-3
48. Römer RA, Römer NS, and Wallis AK. Flexibility and Mobility of SARS-CoV-2-Related Protein Structures. *Scientific Rep* (2021) 11(1). doi:10.1038/s41598-021-82849-2

Conflict of Interest: The authors declare that the research was conducted in the absence of any commercial or financial relationships that could be construed as a potential conflict of interest.

Copyright © 2021 Leong, Voleti and Peng. This is an open-access article distributed under the terms of the Creative Commons Attribution License (CC BY). The use, distribution or reproduction in other forums is permitted, provided the original author(s) and the copyright owner(s) are credited and that the original publication in this journal is cited, in accordance with accepted academic practice. No use, distribution or reproduction is permitted which does not comply with these terms.